PHYSICAL REVIEW D **88,** 013016 (2013)

The shape of spins

Christoph Englert,[1,*] Dorival Gonçalves,[2,3,†] Graeme Nail,[1,‡] and Michael Spannowsky[1,§]
[1]*Department of Physics, Institute for Particle Physics Phenomenology, Durham University, Durham DH1 3LE, United Kingdom*
[2]*Institut für Theoretische Physik, Universität Heidelberg, 69120 Heidelberg, Germany*
[3]*Max-Planck-Institut für Physik, Föhringer Ring 6, 80805 München, Germany*
(Received 15 April 2013; published 26 July 2013)

After the discovery of a Higgs-like particle at the LHC, the determination of its spin quantum numbers across different channels will be the next step in arriving at a more precise understanding of the new state and its role in electroweak symmetry breaking. Event shape observables have been shown to provide extremely sensitive observables for the discrimination of the scalar Higgs boson's $\mathcal{CP}$ quantum numbers as a consequence of the different radiation patterns of Higgs production via gluon fusion vs weak boson fusion in the $pp \to X + 2j$ selection. We show that a similar strategy serves to constrain the spin quantum numbers of the discovered particle as a function of the involved couplings. We also discuss the prospects of applying a similar strategy to future discoveries of Higgs-like particles.

DOI: 10.1103/PhysRevD.88.013016 PACS numbers: 14.80.Bn, 14.80.Ec, 12.60.Cn

I. INTRODUCTION

After the discovery of a Standard Model (SM) Higgs boson-like particle [1] at the LHC [2,3], the measurement its spin is the next step in arriving at a more complete picture of this discovery. There is a theoretical prejudice from Lorentz invariance against spin $J = 1$ [4] as the particle is observed in the decay to photons, which leaves scalar $J = 0$ as the well-defined option in terms of our current understanding of perturbative quantum field theory.

There are well-known phenomenological issues when we analyze $J \geq 2$ hypotheses in perturbative approaches. In particular, there are certain indirect constraints on the spin $J = 2$ options if we take into account the nonobservation of large excesses in $VV + 2j$ final states ($V = W^{\pm}, Z$) at the LHC so far, while there is consistency in $X \to VV$ with the SM within errors. The latter implies that the observed particle is involved in the unitarization of $V_L V_L$ scattering and probably provides the dominant share to the saturation of the unitarity sum rules. In simple realizations, this cannot be achieved with a spin 2 particle [5] and the worsened unitarity problem in longitudinal gauge boson scattering would be manifest in a large cross section in the $VV + 2j$ final state at large invariant masses.

On the other hand, we can perform spin analyses beyond indirect constraints in model-independent ways in the fully reconstructible final states $X \to ZZ$, $\gamma\gamma$ [6–10]. Many of the direct measurement analysis strategies originate from similar questions addressed in hadron physics [11]. Doing so, one typically treats the X decay independent from X production.[1] Indeed, recent LHC measurements along these lines seem to favor $J^{\mathcal{CP}} = 0^+$ searches [13,14].

However, treating the resonance's decay independent from its production does not allow one to draw a more complete picture of Higgs couplings because momentum dependencies are typically encoded in off-shell effects that cannot be studied in this way. It is precisely the momentum dependence of higher-dimensional operators that leaves footprints in the $X + 2j$ channel [15], i.e., the t channel gauge bosons in the weak boson fusion (WBF) topologies are always virtual. In this sense, adapted search strategies for the $X + 2j$ selection not only provide additional sensitivity, which can be used in a global spin hypothesis test across various channels, but also include orthogonal information that cannot be accessed via more traditional spin measurement techniques.

In this paper we show that the global energy flow structure that follows from typical representatives of alternative spin structures provides a highly sensitive observable to study these properties. We select combinations of couplings, right from the beginning, that lead to a SM Higgs-like phenomenology. As Refs. [16–19] explain, the "tagging" jet kinematics in $X + 2j$ final states can be a strong discriminant for the spin of the produced particle X. It should be noted that this typically results from the involved (higher-dimensional) operator structures, which are determined by the spin hypotheses. With this in mind, we specifically analyze spin 2 models that have p_T distributions similar to the SM Higgs [17]. In doing so, we

*christoph.englert@durham.ac.uk
†dorival@mpp.mpg.de
‡graeme.nail@durham.ac.uk
§michael.spannowsky@durham.ac.uk

[1]In the specific case of fermionic final states, however, it is important to take into account the full matrix element in the simulation because, e.g., for a gravitonlike object the only source of deviation from scalar resonances comes from its propagator; see Ref. [12].

complement the analyzes of [16–19] by answering how much sensitivity hides beyond the tagging jet level and how it carries over to experimental reality.

We will also investigate the strategy's prospects for heavier "Higgs" masses. This latter point is motivated by the fact that similar questions, as to those we currently face for the 125 GeV particle, will arise if additional Higgs-like states are discovered in the future. Such states are predicted by many extensions of the SM Higgs sector.

A. Event shapes as electroweak-sensitive observables

The azimuthal angle between the two tagging jets in the $pp \to X + 2j$ selection $\Delta\Phi_{jj}$ [20–24] defined according to rapidity y

$$\Delta\Phi_{jj} = \phi(p_>) - \phi(p_<), \tag{1}$$

where $p^\mu_{\lessgtr} = \sum_{j\in\{\text{jets: } y_j \lessgtr y_X\}} p^\mu_j$, is known to be a highly sensitive observable to the $\mathcal{CP}$ quantum numbers of the produced X state. This finding is not limited to the WBF channels [25] but is known to also work in the gluon fusion channel [24,26]. The latter production mechanism can give rise to $\mathcal{CP}$ odd Higgs production via tree-level $\mathcal{CP}$ odd couplings to the heavy fermion sector (Fig. 1). Such a state is typically present in any nonsinglet Higgs sector extension that features fields transforming in nontrivial representations under $\mathrm{SU}(2)_L$. In light of recent measurements, the fields of these extensions need to be heavier, with suppressed cross sections.

Another way to understand the sensitivity encoded in $\Delta\Phi_{jj}$ is that the amplitude as a whole is sensitive to the $\mathcal{CP}$ quantum numbers. Hence, any additional $\mathcal{CP}$-preserving QCD leg that is attached to diagrams in Fig. 1 will still give rise to an amplitude which encodes the $\mathcal{CP}$-specific properties reflected in $\Delta\Phi_{jj}$ for two-jet configurations. As a result, the entire QCD activity that results from the hard interactions in Fig. 1 can be considered a probe of the produced state X.[2] Finding the "proper" jets of Fig. 1 that reflect the nature of the produced state in a multijet environment amounts to a combinatorial and quantum-interference–governed problem; this results in reduced sensitivity in the $\geq 3j$ selection [20].

A way to circumvent this was outlined in Ref. [17]: Since QCD radiation implies energy-momentum flow, the entire energy distribution in the detector (upon reconstructing and removing X from the list of calorimeter hits) can be expected to provide a superior discriminant compared to $\Delta\Phi_{jj}$ in an inclusive selection. The energy-momentum flow of an LHC event is commonly quantified by means of hadronic event shape observables [27].[3] Indeed, Ref. [29] found an increase in sensitivity that follows from investigating event shapes for discrete $\mathcal{CP}$ measurements.[4] The interplay between event shapes and Higgs physics was further studied in Ref. [30].

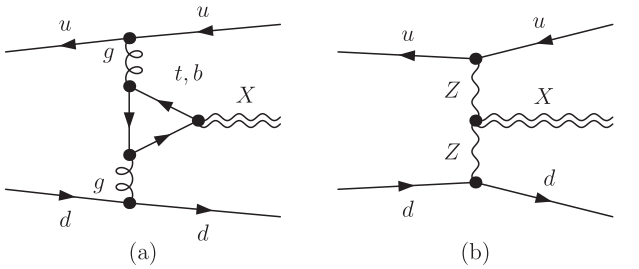

FIG. 1. Sample Feynman diagrams that contribute to $X + 2j$ production via gluon fusion (GF) (a) and WBF (b). We do not show the X decay.

Recently in Refs. [16,17,19] a substantial discriminative power was revealed in the $pp \to X + 2j$ final state for different spin hypotheses $J(X)$. This sensitivity is driven by the energy dependence of operators which mimic the Higgs boson's interactions. The differences in the observed phenomenology can be manifold and depend on the specific higher spin scenario that one investigates. However, a rather generic finding is that spin 1 and 2 operators tend to populate the central region of the detector, thus leading to a departure from a WBF-like signature; consequentially central jet vetoes [31,32] need to be relaxed to be sensitive to such an event topology. This means that backgrounds need to be suppressed by a combination of stiff b vetoes [33] and state-of-the-art signal vs background (S/B) discriminators, such as the matrix element method [34], depending on the final state.[5]

In the following we will consider $pp \to X + 2j$ with X decay to fully leptonic taus for a toy-level signal vs background study to compare the performance of various event shape-based observables. The details of the Higgs reconstruction are inconsequential in this comparison, as all observables are affected in the same way, and the Higgs candidate does not enter our analysis apart from reconstructing the signal within a window cut of 50 GeV around the candidate mass of $m_X \simeq 125$ GeV. Hence, we do not include any tau reconstruction efficiencies that can also vary across the different exclusive tau decay modes [35]. The quality of the Higgs mass reconstruction will eventually rely on a combination of the leptonic and semileptonic

[2]In principle this argument extends also to the soft coherent radiation down to the hadronization scale. These effects are however subleading.

[3]See, e.g., Ref. [28] for publicly available implementations within the RIVET analysis package.

[4]Since the sensitivity does not follow from a specific angular distribution $\Delta\Phi_{jj}$ still remains the observable of choice for mixed $\mathcal{CP}$ states, which can be straightforwardly extracted by fitting trigonometrical functions for an essentially background-free selection [25,26]. This procedure only becomes available at high integrated luminosities.

[5]Another finding of [17,19] is that the sensitivity observed, in the combination of transverse momentum and rapidity difference, points to the invariant dijet mass as a single discriminant.

decay modes with different discovery thresholds due to different S/B ratios.

For demonstration purposes we include the ditau branching ratio to light opposite lepton flavors (6.2%) and assume a perfect tau and Higgs reconstruction in this study. In particular we assume that the full Higgs four momentum can be reconstructed and is known, which straightforwardly allows one to select events in the vicinity of the Higgs mass, thus suppressing the background. The normalization of the latter, however, is the same for all considered observables; hence, possible improvements due to choosing adapted observables should remain independent of the Higgs reconstruction, as long as the Higgs boson can be identified in the particular final state, i.e., when the signal can be dug out from the background in the first place as demonstrated in [36–38].

Our analysis strategy is also insensitive to the specifics of the ''Higgs'' decay channel, and our methods straightforwardly generalize to other decay channels such as, e.g., the $\gamma\gamma + 2j$ selection.

II. ANALYSIS SETUP

For the purpose of comparability, we closely follow Ref. [29]. We model our signal hypotheses with a combination of MADGRAPH [39] and HERWIG++ [40]. For the simulation of the backgrounds we generate matched events with SHERPA [41] and in the following limit ourselves to the $t\bar{t}$ + jets and Zjj backgrounds [25], normalizing these event samples to the next-to-next-to-leading-order-inclusive $t\bar{t}$ [42,43] and next-to-leading-order Zjj cross sections [44–46]. All the simulations in this section and in what follows we perform for an LHC energy of 14 TeV.

We apply a typical WBF selection [25,29] and cluster jets with the anti-kT algorithm [47] as implemented in FASTJET [48] with $D = 0.4$ and define jets with the thresholds

$$p_{T,j} \geq 40 \text{ GeV} \quad \text{and} \quad |y_j| \leq 4.5. \tag{2}$$

We impose an invariant mass cut on the two hardest jets (tagging jets) in the event of

$$m_{jj} = \sqrt{(p_{j,1} + p_{j,2})^2} \geq 600 \text{ GeV} \tag{3}$$

and reconstruct the Higgs from taus with

$$p_\tau \geq 20 \text{ GeV} \quad \text{and} \quad |\eta_\tau| \leq 2.5 \tag{4}$$

within a 50 GeV window around 125 GeV. The Higgs candidate has to fall between the tagging jets

$$\min(y_1, y_2) < y_X < \max(y_1, y_2). \tag{5}$$

We further suppress the $t\bar{t}$ + jets background by imposing a central b veto with an efficiency of 80% [33]. The additional signal reduction due to mistagging is negligible, at most a few percent [33], within the approximations we make. When normalizing *all signal samples to the SM Higgs cross section* after cuts (i.e., we treat the $J = 2$ hypotheses as Higgs lookalikes) we have signal cross sections $\sigma(X + 2j) = 3.82$ fb. The combined background is $\sigma(\text{bkg}) = 6.54$ fb.[6]

We proceed further by setting up two different track selections that eventually enter the evaluation of the considered event shape observables. One of which is more robust against pileup that can cause issues when we want to study the global event properties in the context of this paper.

(i) For the events that pass the above selection criteria we feed all calorimeter hits with $p_T \geq 1$ GeV and $|\eta| \leq 4.5$ into the definition of the event shapes. This amounts to the most inclusive definition of the event shapes that is possible in the light of the above cuts. Selecting events according to the requirements Eqs. (2)–(5) is somewhat at odds with so-called continuous globalness [27], which guarantees good resummation properties. This has no effect on the validity of the event shapes definition on the particular final state; yet QCD resummation is not as straightforward anymore as for inclusive QCD events. This shortcoming is also present in other jet-based observables, e.g., in $\Delta\Phi_{jj}$. However, the used selection is the most inclusive possible in the light of unavoidable signal vs background discrimination. To this end, we note that the analysis of Ref. [27] also shows that matched shower Monte Carlos reproduce the analytically resummed results well, so that we can expect our simulation to be under sufficient control. Quite obviously, this selection will be affected by pileup activity.

(ii) The pileup conditions for $\sqrt{s} = 14$ TeV will need to be assessed when the LHC turns on again, but it can be expected that pileup suppression in the central part of the detector is going to allow to lower jet thresholds in the rapidity region of the tracker $|\eta| \leq 2.5$ [49]. Currently, there is no tracking available for the more forward rapidity regions, so we will need to rely on hard jets to reduce in- and out-of-time pileup and underlying event.
To reflect the effect of pileup suppression to achieve a more robust definition of our observables we modify our event selection. We cluster jets as before, with the anti-kT algorithm and $D = 0.4$, but this time we use the constituents of the jets obeying

$$p_{T,j} \geq \begin{cases} 40 \text{ GeV}, & 2.5 < |\eta_j| \leq 4.5, \\ 10 \text{ GeV}, & |\eta_j| \leq 2.5 \end{cases} \tag{6}$$

as input for the event shapes instead of all particle tracks as considered in (i). While we require hard jets in the forward region, in the central region of the detector we allow a lower optimistic p_T cut on the jets. In the central region pileup contribution can be

[6]The details of the cutflow are identical to Ref. [29] and can be found in this earlier publication.

reduced using information from the tracker. Other methods to enhance pileup suppression are possible too, e.g., using the approach of Ref. [50]. We stress that the feasibility of such a procedure needs to be validated by the experiments: The more inclusive the realistic selection is allowed to be, the more superior the performance of the event shapes will turn out. Furthermore, we explicitly require additional jet activity (specifically $n_j \geq 3$) which probes the spin structure induced radiation pattern. Since we are requiring at least three jets according to these modified criteria, the sensitivity we will find can be straightforwardly enhanced by including sensitivity from $\Delta\Phi_{jj}$, $\Delta\eta_{jj}$, p_{T_j} (or equivalently m_{jj}) for the *exclusive* two jet category [17] in a hybrid observable approach. We find cross sections for these cuts of $\sigma(\text{signal}) = 1.89$ fb, while the background remains unchanged.[7]

For the spin 2 hypothesis

$$\mathcal{L}_2 = -g_1 G_{\mu\nu} T_V^{\mu\nu} - g_2 G_{\mu\nu} T_G^{\mu\nu} - g_3 G_{\mu\nu} T_f^{\mu\nu}, \quad (7)$$

where $G_{\mu\nu}$ is the spin 2 resonance and $T^{\mu\nu}_{V,G,f}$ is the energy-momentum tensor for the electroweak gauge bosons, gluons and fermions, we consider two representative scenarios [17].

2^+.—The ordinary gravitonlike tensor particle paradigm (i.e., $g_1 = g_2 = g_3 = 1/\Lambda$), as considered in many other publications (see, e.g., Refs. [16,51]), has jet kinematics in the $X + 2j$ final state that are close to the SM Higgs, once the additional selection cuts are imposed [17]. The tagging jets are well separated in η and their p_T distribution is not too different from the SM Higgs boson.

$2^+_{\text{ew+q}}$.—We also study a model which has considerably harder jets while the WBF rapidity gap (and hence WBF-likeness) is still preserved. This specific model constrains the tensor couplings to weak bosons and fermions (i.e., $g_1 = g_3 = 1/\Lambda$ and $g_2 = 0$). This specific operator selection is therefore a less "reasonable" representative of a spin 2 Higgs lookalike.

Our two choices will be clear from the discussion below and are also motivated by our findings for heavier Higgs-like particles in Sec. III.

The results of a number of event shape observables (for their definition we refer the reader to the Appendix and Ref. [27]) are depicted in Fig. 2 for selection (i). This figure should be compared to Fig. 3, which displays the same distributions subject to the modified requirements (ii).

To quantify the statistical discriminative power of the event shape observables we perform a binned log-likelihood hypothesis test [52] in Figs. 4 and 5; this provides a statistically well-defined estimate of the luminosity (upon dividing out all reconstruction efficiencies) that is required to reject the spin 2 hypotheses at the 5 sigma level using the CL_S method [53].

The results of this analysis are shown in Fig. 4 for the $2^+_{\text{ew+q}}$ and in Fig. 5 for the 2^+ cases. As already expected from Figs. 2 and 3, the broadening observables perform best. Depending on the specific scenario, these observables are robust against pileup as discussed in (ii). Figure 5, however, also shows that, when the jet kinematics become SM-like, this will be reflected in a lower sensitivity of the event shapes to the involved spin hypothesis. This especially holds when discriminative power at smaller broadening is lost due to soft radiation not taken into account for selection (ii) vs (i). The latter point also explains our initial choice of the spin 2 hypotheses: 2^+ is characterized by soft radiation and therefore suitable to be studied using event shape observables. We find broadening observables to provide the strongest statistical sensitivity. However, while this model can be formidably constrained using event shapes if pileup is under sufficient control, i.e., when the actual selection can be chosen closer to (i), the discriminative power of the broadening observables is severely reduced for selection (ii). On the other hand, $2^+_{\text{ew+q}}$ which has a slightly harder spectrum is robust in our comparison (i) vs (ii) and the event shape observables provide a statistically appealing single-valued discriminant.

III. SPIN DISCRIMINATION OF FUTURE HIGGS-LIKE RESONANCES

Let us finally comment on the prospect of using the methods of the previous section also in the context of spin analyses of Higgs-like states that might be discovered in the future with a heavier mass. This is not immediately clear since the higher mass scale implies a different (soft) radiation pattern. As a representative example we discuss $m_X \simeq 300$ GeV.

In general we can expect relatively small couplings of this additional state to the electroweak gauge bosons Z and W, as current measurements seem to suggest that unitarity cancellations, which characteristically determine the couplings of additional massive scalars with corresponding couplings, are saturated by the 125 GeV state. The standard technique in $X \to ZZ$ [10,54] might hence not be applicable and an investigation of the $X + 2j$ final state could well be the only phenomenologically available channel to constrain the spin and $\mathcal{CP}$ structure of such a discovery.

We consider these reasons as enough motivation to limit ourselves for scalar boson candidates to the GF channel [Fig. 1(a)]. For the spin 2 candidates we will again adopt the scenarios of the previous section, which will have quite different phenomenology as compared to the $m_X = 125$ GeV case.

For spin 1 candidates our above arguments constrain the interactions of copies of the SM gauge bosons. The phenomenology of a Kaluza-Klein excitation spectrum as

[7]Note that this motivated central jet vetoes (CJV) [31,32] in the first place. The sensitivity we are going to find is lost in employing CJV-bases analysis strategies.

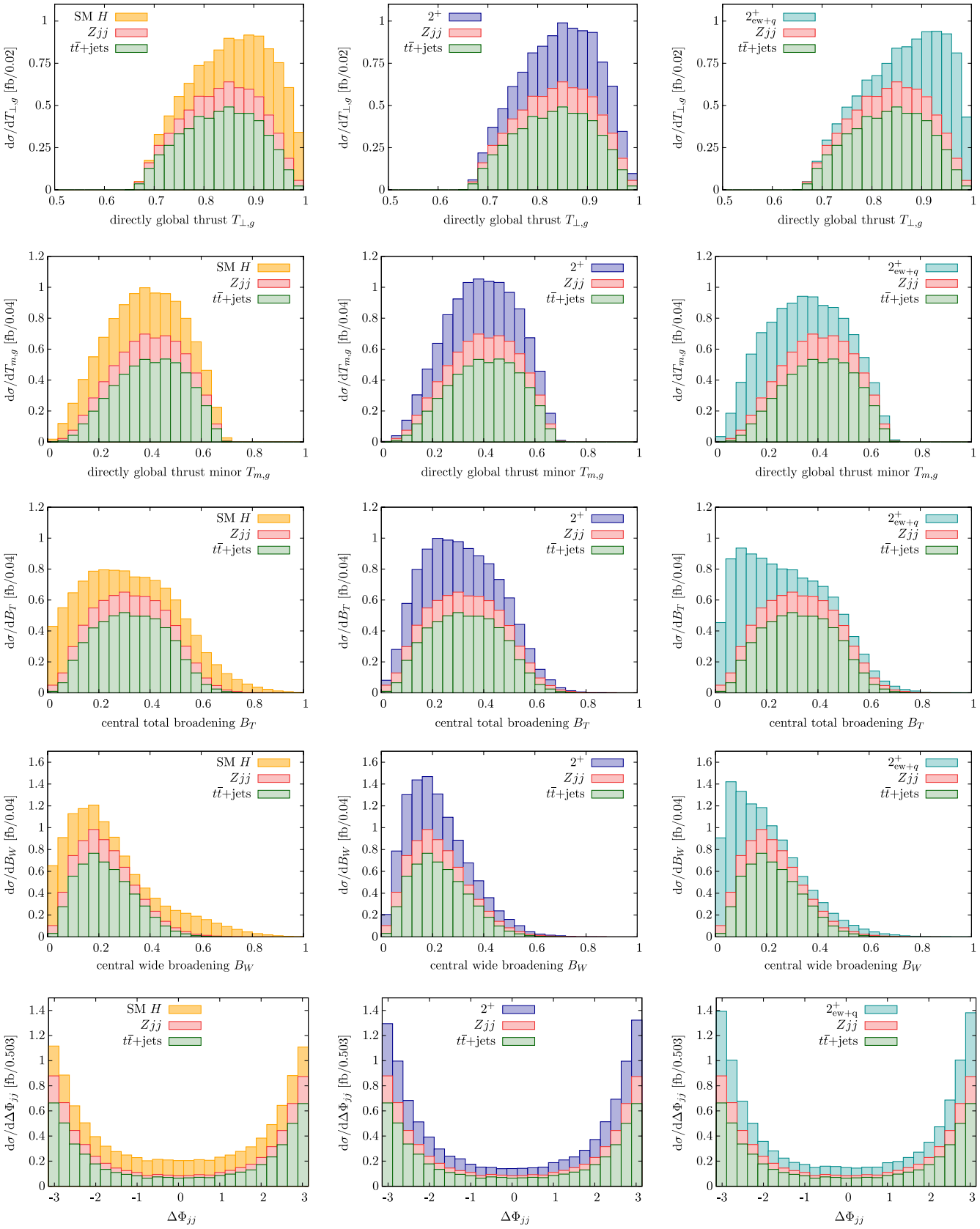

FIG. 2 (color online). Event shape distribution for the different event shapes calculated from all particle tracks in $|\eta| < 4.5$ with $p_T \geq 1$ GeV for selection (i). We also show $\Delta\Phi_{jj}$. The ditau branching ratio to light opposite lepton flavors (6.2%) is included and we assume a perfect tau reconstruction efficiency for demonstration purposes.

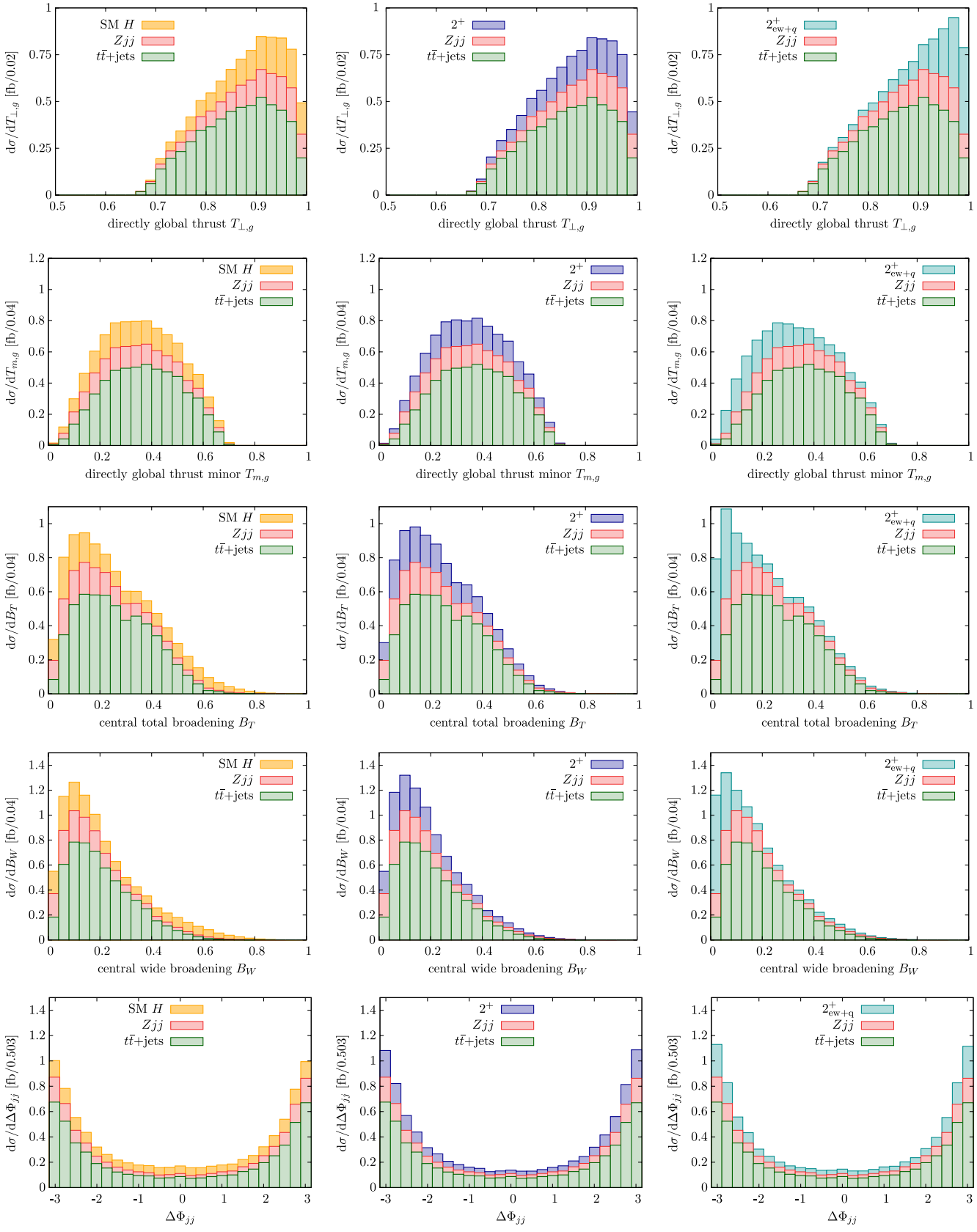

FIG. 3 (color online). Event shape distribution calculated from jet constituents of selection (ii). We also show $\Delta\Phi_{jj}$. The ditau branching ratio to light opposite lepton flavors (6.2%) is included and we assume a perfect tau reconstruction efficiency for demonstration purposes.

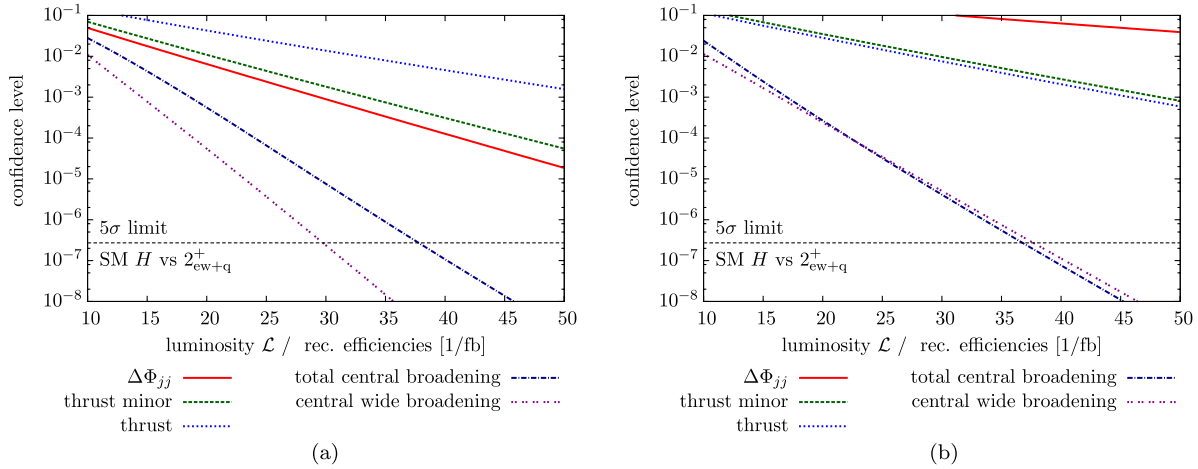

FIG. 4 (color online). Result of the binned log-likelihood hypotheses test for the distinction between the SM H and $2^+_{\mathrm{ew+q}}$ hypotheses. (a) Cut scenario (i). (b) Cut scenario (ii).

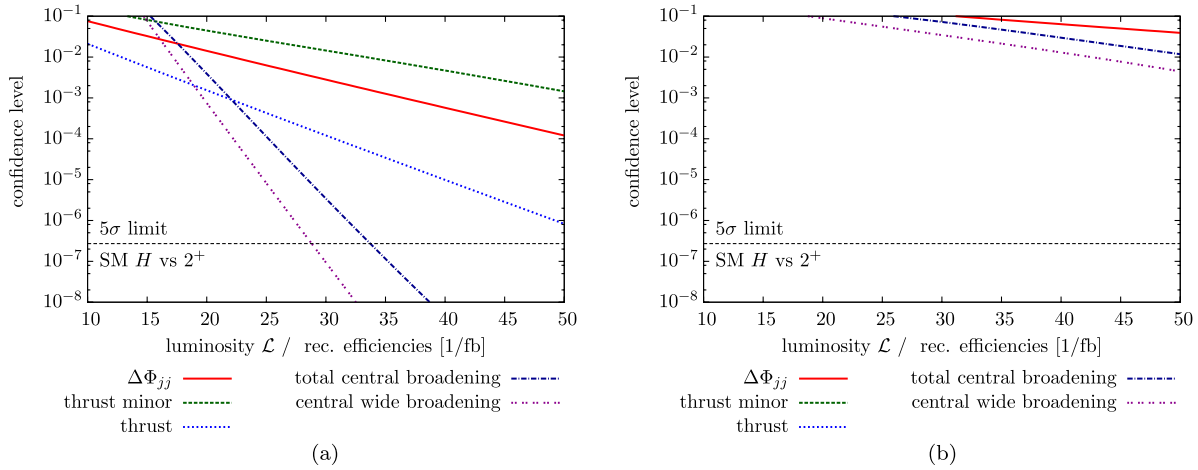

FIG. 5 (color online). Result of the binned log-likelihood hypotheses test for the distinction between the SM H and 2^+ hypotheses. (a) Cut scenario (i). (b) Cut scenario (ii).

encountered in, e.g., warped extra dimensions (and their dual interpretation as vectorial and axial vector resonances of a strongly interacting sector) is therefore heavily suppressed in the SM vector boson final states. There is an exception to the unitarity argument which are $Z'ZZ$ interactions as determined in the generalized Landau Yang theorem [55]. The structure of the interaction vertices does not introduce an energy-dependent unitarity violation and, hence, is not constrained by current measurements. We include this interaction to model a WBF [Fig. 1(b)] spin 1 candidate $J(X) = 1^-_Z$.

Gluon-fusion contributions for spin 1 degrees of freedom analogous to Fig. 1(a) are more difficult to model. Furry's theorem [56] guarantees the exact cancellation of vector current from $J^{\mathcal{CP}}(X) = 1^-$ hypothesis in $gg \to X$. Axial vector currents still have to obey the Landau Yang theorem [4]. This renders an observation of prompt gluon fusion impossible; on-shell production exactly vanishes and gluon fusion becomes a function of the $J^{\mathcal{CP}}(X) = 1^+$ particle's width and the virtuality of the gluon. These small effects are at odds with conventional bump searches and leave gluon fusion, as depicted in Fig. 1(a), as the only production mechanism when such a state has suppressed couplings to the SM Z's (these couplings are again determined by the generalized Landau Yang theorem). While the particle X, in Fig. 1(a), can be considered on shell for resonance-driven searches, the t channel gluons are always off shell: This enables $J^{\mathcal{CP}}(X) = 1^+$ production via gluon fusion (see also Ref. [57]). For the moment we are not interested in a survey of the effects of $d > 6$ operators that are involved in these interactions [58] on the events' energy momentum flow. We however note that different effective operators will contribute to the gluon-gluon, gluon-quark, and quark-quark channels.

Instead, we will toy model axial vector particles in gluon fusion plus two jets by introducing a doublet of heavy

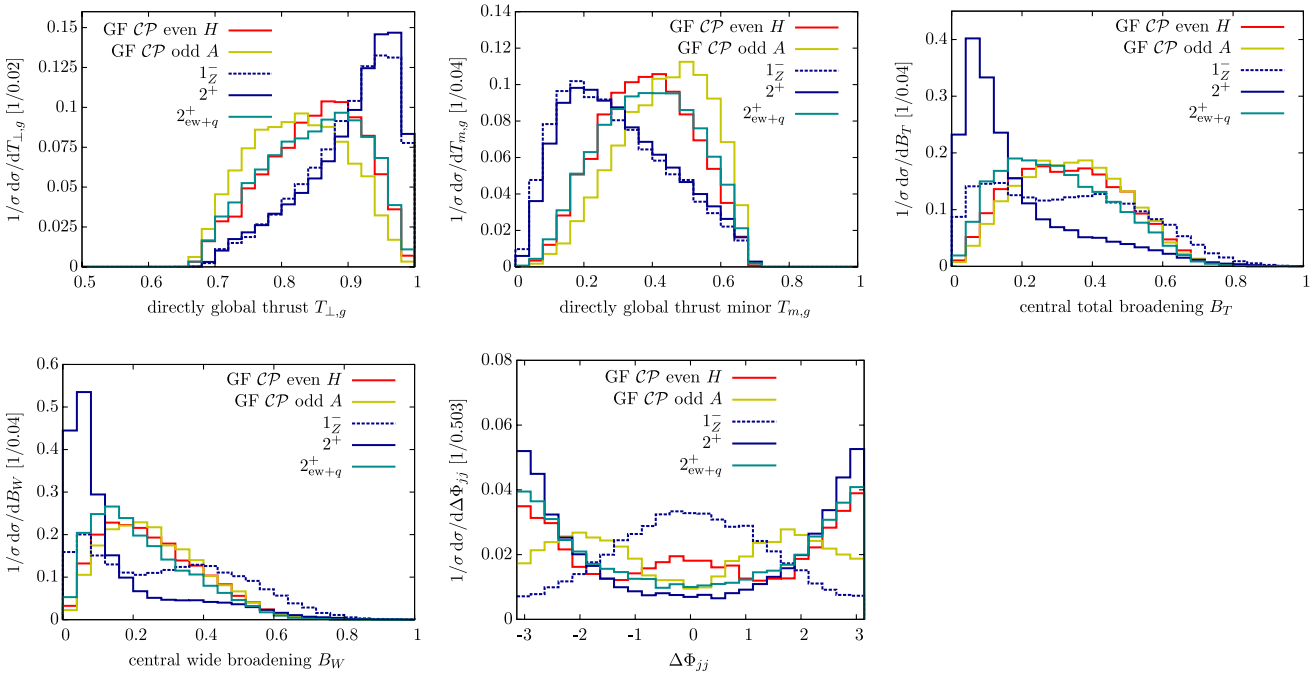

FIG. 6 (color online). Event shape and Φ_{jj} distributions for selection (i) and $m_X = 300$ GeV. As depicted in Fig. 1(a), the label GF stands for the gluon fusion production.

fermions, $m_{b'} = 1$ TeV, $m_{t'} = 2$ TeV, which couple to the axial vector boson with couplings chosen such that anomaly cancellation is manifest: $g_L(b') + g_R(b') = 0 = g_R(t') + g_R(b') - g_L(t') - g_L(b')$. Analytic cross-checks have been performed using FEYNARTS/FORMCALC/LOOPTOOLS [59] and we find a dependence of the amplitude on only $g_R(b')$, whose size is unimportant for the shape comparisons we perform in the following. We keep the full mass dependence by simulating $qq' \to 1_{\mathrm{q}}^+ + qq'$ events with a modified version of MADGRAPH v4.4 [60] that links a customized one-loop capable HELAS [61] library, which is based on the LOOPTOOLS/FF packages [59,62].

To gain a qualitative picture we compare the energy-momentum flow of this model against the corresponding full one-loop SM Higgs events $qq' \to 0_{\mathrm{SM}}^+ + qq'$.

The (normalized) results are presented in Fig. 6 for the identical jet cut setup of Sec. II. We do not include the backgrounds as these depend on the specific decay channel in which such a future resonance will be discovered. Typical QCD background suppression will however always be centered around the cuts of the previous section, independent of the specific exclusive decay channel of X. From the shown distributions it is clear that there is substantial discriminative power in separating the scalar options from 1_Z^- and 2^+ in the event shape observables. A combination with ordinary jet-based observables such as $\Delta\Phi_{jj}$ will serve to discriminate these options further for tighter selections if feasible.

In Fig. 7 we finally show the comparison of the quark channels for the 0^+ vs 1_{q}^+, which also provides insights into how different partonic channels (and hence effective operators) will influence our findings.

The gluonic initial states will typically radiate more and influence the final state radiation pattern; this is visible in

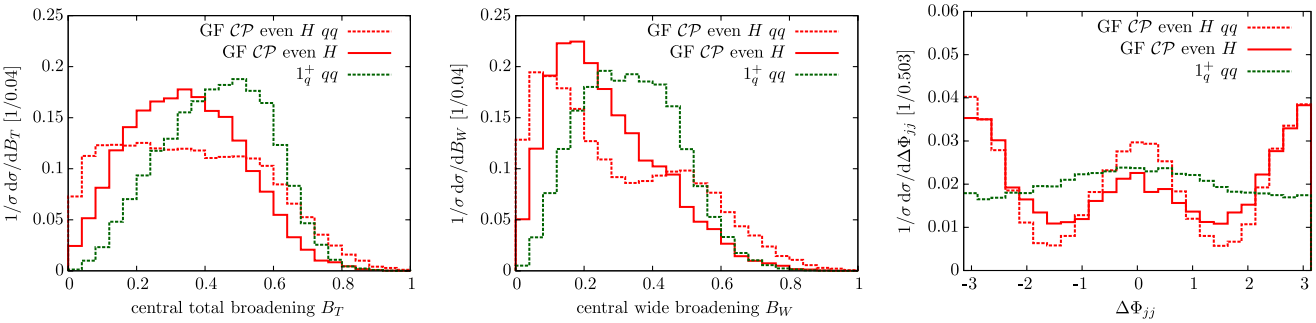

FIG. 7 (color online). Event shape comparison for the 0^+ and 1_q^+ for the qq'-induced channels including the full mass dependence $m_X = 300$ GeV. As depicted in Fig. 1(a), the label GF stands for the gluon fusion production.

Fig. 7. This underlines the fact that measurements in the $X + 2j$ channel are momentum and, hence, model dependent as already mentioned in the introduction [16,17,19]. Note also that our spin 2 hypotheses behave completely opposite compared to the $m_h = 125$ GeV case due to the changed momentum dependence of the cross section on the tagging jets.

Hence, the $2^+_{\mathrm{ew+q}}$ is a more "Higgs-like" alternative hypothesis when such an analysis is performed in the future after a heavy Higgs-like object has potentially been discovered. This comes at the price of a significantly weaker discrimination which requires large integrated luminosities.

IV. SUMMARY AND CONCLUSIONS

The recent discovery of a Higgs-like particle at the LHC and further measurements of it seem to suggest that we have indeed discovered a particle which is consistent with the $J^{\mathcal{CP}}(X) = 0^+$ SM Higgs boson prediction. Analyses with increased statistics across many different channels will allow one to answer the $J^{\mathcal{CP}}$ question more reliably. The $pp \to X + 2j$ mode, when analyzed in inclusive selections, provides a valuable channel to discriminate between different spin (and $\mathcal{CP}$) hypotheses when the events' global QCD energy-momentum flow pattern is analyzed. The latter is most efficiently captured in event shape distributions. How inclusive the $pp \to X + 2j$ selection can eventually be depends highly on the involved experimental systematics, and this should be addressed by the LHC experiments. While thrust provides a straightforward handle to discriminate discrete $\mathcal{CP}$ values [29], the broadening observables reflect the spin-induced radiation patterns. Issues that may arise from challenging pileup conditions can be counteracted with adopted definitions of the event shape observables and hybrid exclusive and inclusive definitions of the employed single-valued discriminants. Depending on the spin 2 scenario (no spin 2 scenario is theoretically motivated but merely invoked as an alternative hypothesis to be excluded) we find large discriminative power in the accompanied energy-momentum flow. This generalizes the results of Refs. [16,17,19,29]. Pileup, as for many analyses, can become a challenge of the discussed analysis strategy to the point where discriminative power in all collider observables is lost in the $X + 2j$ final state. This again highly depends on the chosen hypothesis.

Given the consistency of the observed cross sections in $pp \to X \to ZZ,\ W^+W^-$ with the SM Higgs boson, it is likely that spin analyses of an additional resonance as predicted by many Beyond the Standard Model scenarios cannot be straightforwardly performed in the $X \to \gamma\gamma, ZZ$ channels. In this case an event shape-based analysis of the QCD energy-momentum flow might be crucial since it does not rely on a particular exclusive final state decay of X. Indeed, we find significant discriminative power of the event shape observables for heavier "Higgs" masses, which allows one to discriminate various $J^{\mathcal{CP}}$ hypotheses in combination with exclusive 2-jet measurements in the same channel [17]. As shown in this work, the advantages of event shape-based analyses are not limited to the study of pure QCD events but clearly generalize to the interplay of QCD with the (BSM) electroweak sector.

ACKNOWLEDGMENTS

We thank Andrea Banfi, Gavin Salam, and Giulia Zanderighi for providing the CAESAR event shape library. C. E. acknowledges funding by the Durham International Junior Research Fellowship scheme.

APPENDIX: DEFINITIONS OF THE STUDIED EVENT SHAPES

Event shapes are widely used observables to investigate geometrical properties of particle collisions at lepton and hadron colliders [63–67], which can be described to very high theoretical accuracy; see, e.g., [27,67]. At hadron colliders one typically defines the observables in the beam transverse plane. *Transverse thrust* is therefore defined as the maximization procedure in the transverse plane

$$T_{T,g} = \max_{\mathbf{n}_T} \frac{\sum_i |\mathbf{p}_{T,i} \cdot \mathbf{n}_T|}{\sum_i |\mathbf{p}_{T,i}|}, \qquad |\mathbf{n}_T| = 1, \tag{A1}$$

where $\mathbf{p}_{T,i}$ denotes the transverse momentum of the track i. The transverse thrust value of circularly symmetric event is $T_{T,g} = 2/\pi \simeq 0.64$, while an ideal alignment is characterized by $T_{T,g} = 1$.

As a result of the maximization procedure we obtain the transverse thrust axis $\mathbf{n}_T$ which enters the definition of transverse *thrust minor*

$$T_{m,g} = \frac{\sum_i |\mathbf{p}_{T,i} \times \mathbf{n}_T|}{\sum_i |\mathbf{p}_{T,i}|}, \tag{A2}$$

which measures the energy-momentum flow perpendicular to the transverse thrust axis.

Observables that are particularly helpful in the context of spin analyses are broadening observables [65]. For their definitions we first specify a central region C in terms of pseudorapidity; here C corresponds to $|\eta| \leq 4.5$. Then we split this region according to transverse thrust axis

$$\text{region} \begin{matrix} C_U \\ C_D \end{matrix} \quad \mathbf{p}_{T,i} \cdot \mathbf{n}_T \gtrless 0 \tag{A3a}$$

and subsequently compute the weighted pseudorapidity and azimuthal angle

$$\eta_\sigma = \frac{\sum_i |\mathbf{p}_{T,i}| \eta_i}{\sum_i |\mathbf{p}_{T,i}|}, \qquad \phi_\sigma = \frac{\sum_i |\mathbf{p}_{T,i}| \phi_i}{\sum_i |\mathbf{p}_{T,i}|}, \qquad \sigma = C_U, C_D. \tag{A3b}$$

The broadening of the above regions is then defined as

$$B_\sigma = \frac{1}{2Q_T}\sum_{i\in\sigma}|\mathbf{p}_{T,i}|\sqrt{(\eta_i-\eta_\sigma)^2+(\phi_i-\phi_\sigma)^2}, \qquad \sigma = C_U, C_D \tag{A3c}$$

with $Q_T = \sum_i |\mathbf{p}_{T,i}|$. The *central total broadening* and *central wide broadening* observables are, respectively,

$$\text{central total broadening: } B_T = B_{C_U} + B_{C_D}, \qquad \text{central wide broadening: } B_W = \max\{B_{C_U}, B_{C_D}\}. \tag{A3d}$$

[1] P. W. Higgs, Phys. Lett. **12**, 132 (1964); Phys. Rev. Lett. **13**, 508 (1964); F. Englert and R. Brout, Phys. Rev. Lett. **13**, 321 (1964); G. S. Guralnik, C. R. Hagen, and T. W. B. Kibble, Phys. Rev. Lett. **13**, 585 (1964).

[2] ATLAS Collaboration, Phys. Lett. B **716**, 1 (2012); Report No. ATLAS-CONF-2012-170.

[3] CMS Collaboration, Phys. Lett. B **716**, 30 (2012); Report No. CMS-PAS-HIG-12-045.

[4] L. F. Landau, Dokl. Akad. Nauk SSSR **60**, 207 (1948); C. N. Yang, Phys. Rev. **77**, 242 (1950).

[5] A. Alboteanu, W. Kilian, and J. Reuter, J. High Energy Phys. 11 (2008) 010.

[6] Y. Gao, A. V. Gritsan, Z. Guo, K. Melnikov, M. Schulze, and N. V. Tran, Phys. Rev. D **81**, 075022 (2010); A. De Rujula, J. Lykken, M. Pierini, C. Rogan, and M. Spiropulu, Phys. Rev. D **82**, 013003 (2010).

[7] S. Y. Choi, M. M. Muhlleitner, and P. M. Zerwas, Phys. Lett. B **718**, 1031 (2013).

[8] J. Ellis and D. S. Hwang, J. High Energy Phys. 09 (2012) 071.

[9] A. Alves, Phys. Rev. D **86**, 113010 (2012).

[10] D. J. Miller, S. Y. Choi, B. Eberle, M. M. Muhlleitner, and P. M. Zerwas, Phys. Lett. B **505**, 149 (2001); S. Y. Choi, D. J. Miller, M. M. Muhlleitner, and P. M. Zerwas, Phys. Lett. B **553**, 61 (2003); C. P. Buszello, I. Fleck, P. Marquard, and J. J. van der Bij, Eur. Phys. J. C **32**, 209 (2004).

[11] N. Cabibbo and A. Maksymowicz, Phys. Rev. **137**, B438 (1965); **168**, 1926(E) (1968); T. L. Trueman, Phys. Rev. D **18**, 3423 (1978); J. R. Dell'Aquila and C. A. Nelson, Phys. Rev. D **33**, 80 (1986).

[12] S. Banerjee, J. Kalinowski, W. Kotlarski, T. Przedzinski, and Z. Was, Eur. Phys. J. C **73**, 2313 (2013).

[13] ATLAS Collaboration, Report No. ATLAS-CONF-2013-029; ATLAS Collaboration, Report No. ATLAS-CONF-2013-031; CMS Collaboration, Report No. CMS-PAS-HIG-13-002.

[14] A. Djouadi and G. Moreau, arXiv:1303.6591.

[15] V. Hankele, G. Klamke, D. Zeppenfeld, and T. Figy, Phys. Rev. D **74**, 095001 (2006).

[16] J. Frank, M. Rauch, and D. Zeppenfeld, Phys. Rev. D **87**, 055020 (2013).

[17] C. Englert, D. Goncalves-Netto, K. Mawatari, and T. Plehn, J. High Energy Phys. 01 (2013) 148.

[18] V. A. Khoze, W. J. Stirling, and P. H. Williams, Eur. Phys. J. C **31**, 91 (2003).

[19] A. Djouadi, R. M. Godbole, B. Mellado, and K. Mohan, Phys. Lett. B **723**, 307 (2013).

[20] J. R. Andersen, K. Arnold, and D. Zeppenfeld, J. High Energy Phys. 06 (2010) 091.

[21] K. Hagiwara, Q. Li, and K. Mawatari, J. High Energy Phys. 07 (2009) 101.

[22] V. Del Duca, W. Kilgore, C. Oleari, C. R. Schmidt, and D. Zeppenfeld, Phys. Rev. D **67**, 073003 (2003).

[23] F. Campanario, M. Kubocz, and D. Zeppenfeld, Phys. Rev. D **84**, 095025 (2011).

[24] T. Figy, C. Oleari, and D. Zeppenfeld, Phys. Rev. D **68**, 073005 (2003); T. Figy and D. Zeppenfeld, Phys. Lett. B **591**, 297 (2004); V. Del Duca, G. Klamke, D. Zeppenfeld, M. L. Mangano, M. Moretti, F. Piccinini, R. Pittau, and A. D. Polosa, J. High Energy Phys. 10 (2006) 016; J. M. Campbell, R. K. Ellis, and G. Zanderighi, J. High Energy Phys. 10 (2006) 028.

[25] T. Plehn, D. L. Rainwater, and D. Zeppenfeld, Phys. Rev. Lett. **88**, 051801 (2002).

[26] G. Klamke and D. Zeppenfeld, J. High Energy Phys. 04 (2007) 052.

[27] A. Banfi, G. P. Salam, and G. Zanderighi, J. High Energy Phys. 06 (2010) 038; 01 (2002) 01; 08 (2004) 062.

[28] A. Buckley *et al.*, arXiv:1003.0694.

[29] C. Englert, M. Spannowsky, and M. Takeuchi, J. High Energy Phys. 06 (2012) 108.

[30] C. Bernaciak, M. S. A. Buschmann, A. Butter, and T. Plehn, Phys. Rev. D **87**, 073014 (2013).

[31] Y. L. Dokshitzer, S. I. Troian, and V. A. Khoze, Yad. Fiz. **46**, 1220 (1987) [Sov. J. Nucl. Phys. **46**, 712 (1987)]; Y. L. Dokshitzer, V. A. Khoze, and T. Sjostrand, Phys. Lett. B **274**, 116 (1992); J. D. Bjorken, Phys. Rev. D **47**, 101 (1993).

[32] U. Baur and E. W. N. Glover, Phys. Lett. B **252**, 683 (1990); V. D. Barger, K.-m. Cheung, T. Han, and D. Zeppenfeld, Phys. Rev. D **44**, 2701 (1991); **48**, 5444(E) (1993); D. L. Rainwater, R. Szalapski, and D. Zeppenfeld, Phys. Rev. D **54**, 6680 (1996); B. E. Cox, J. R. Forshaw, and A. D. Pilkington, Phys. Lett. B **696**, 87 (2011); S. Ask, J. H. Collins, J. R. Forshaw, K. Joshi, and A. D. Pilkington, J. High Energy Phys. 01 (2012) 018.

[33] See, e.g., ATLAS Collaboration, Report No. ATLAS-CONF-2012-043.

[34] K. Kondo, J. Phys. Soc. Jpn. **57**, 4126 (1988); D. E. Soper and M. Spannowsky, Phys. Rev. D **84**, 074002 (2011); J. M. Campbell, W. T. Giele, and C. Williams, J. High Energy Phys. 11 (2012) 043; J. R. Andersen, C. Englert, and M. Spannowsky, Phys. Rev. D **87**, 015019 (2013); A. Freitas and J. S. Gainer, Phys. Rev. D **88**, 017302 (2013); J. M. Campbell, R. K. Ellis, W. T. Giele, and C. Williams, Phys. Rev. D **87**, 073005 (2013).

[35] CMS Collaboration, Report No. CMS-PAS-TAU-11-001, 2011.

[36] M. Heldmann and D. Cavalli, Report No. ATL-PHYS-PUB-2006-008; Report No. ATL-COM-PHYS-2006-010.

[37] CMS Collaboration, Phys. Lett. B **713**, 68 (2012).

[38] ATLAS Collaboration, Report No. ATLAS-CONF-2012-160; CMS Collaboration, Report No. CMS-HIG-13-004.

[39] J. Alwall, M. Herquet, F. Maltoni, O. Mattelaer, and T. Stelzer, J. High Energy Phys. 06 (2011) 128.

[40] M. Bahr *et al.*, Eur. Phys. J. C **58**, 639 (2008).

[41] T. Gleisberg, S. Hoeche, F. Krauss, M. Schonherr, S. Schumann, F. Siegert, and J. Winter, J. High Energy Phys. 02 (2009) 007; S. Schumann and F. Krauss, J. High Energy Phys. 03 (2008) 038; T. Gleisberg and S. Hoeche, J. High Energy Phys. 12 (2008) 039; S. Hoeche, F. Krauss, S. Schumann, and F. Siegert, J. High Energy Phys. 05 (2009) 053.

[42] P. Nason, S. Dawson, and R. K. Ellis, Nucl. Phys. **B327**, 49 (1989); **B335**, 260(E) (1990); W. Beenakker, W. L. van Neerven, R. Menge, G. A. Schuler, and J. Smith, Nucl. Phys. **B351**, 507 (1991); M. L. Mangano, P. Nason, and G. Ridolfi, Nucl. Phys. **B373**, 295 (1992); S. Frixione, M. L. Mangano, P. Nason, and G. Ridolfi, Phys. Lett. B **351**, 555 (1995).

[43] S. Moch and P. Uwer, Nucl. Phys. B, Proc. Suppl. **183**, 75 (2008); P. Baernreuther, M. Czakon, and A. Mitov, Phys. Rev. Lett. **109**, 132001 (2012); M. Czakon and A. Mitov, J. High Energy Phys. 12 (2012) 054; M. Czakon, P. Fiedler, and A. Mitov, Phys. Rev. Lett. **110**, 252004 (2013).

[44] J. M. Campbell and R. K. Ellis, Nucl. Phys. B, Proc. Suppl. **205–206**, 10 (2010); R. K. Ellis, Nucl. Phys. B, Proc. Suppl. **160**, 170 (2006).

[45] K. Arnold *et al.*, Comput. Phys. Commun. **180**, 1661 (2009).

[46] J. Campbell and R. K. Ellis, Phys. Rev. D **65**, 113007 (2002); C. Oleari and D. Zeppenfeld, Phys. Rev. D **69**, 093004 (2004).

[47] M. Cacciari, G. P. Salam, and G. Soyez, J. High Energy Phys. 04 (2008) 063.

[48] M. Cacciari, G. P. Salam, and G. Soyez, Eur. Phys. J. C **72**, 1896 (2012).

[49] CMS Collaboration, Report No. CMS PAS PFT-09/001.

[50] G. Soyez, G. P. Salam, J. Kim, S. Dutta, and M. Cacciari, Phys. Rev. Lett. **110**, 162001 (2013).

[51] J. Ellis, D. S. Hwang, V. Sanz, and T. You, J. High Energy Phys. 11 (2012) 134; C.-Q. Geng, D. Huang, Y. Tang, and Y.-L. Wu, Phys. Lett. B **719**, 164 (2013); J. Ellis, R. Fok, D. S. Hwang, V. Sanz, and T. You, arXiv:1210.5229; J. Ellis, V. Sanz, and T. You, arXiv:1211.3068; T. Modak, D. Sahoo, R. Sinha, and H.-Y. Cheng, arXiv:1301.5404.

[52] T. Junk, Nucl. Instrum. Methods Phys. Res., Sect. A **434**, 435 (1999); CDF Note 8128; CDF Note 7904; H. Hu and J. Nielsen, in Proceedings of the First Workshop on Confidence Limits, CERN, 2000 (unpublished).

[53] A. L. Read, Report No. CERN-OPEN-2000-205; J. Phys. G **28**, 2693 (2002).

[54] C. Hackstein and M. Spannowsky, Phys. Rev. D **82**, 113012 (2010); C. Englert, C. Hackstein, and M. Spannowsky, Phys. Rev. D **82**, 114024 (2010).

[55] W.-Y. Keung, I. Low, and J. Shu, Phys. Rev. Lett. **101**, 091802 (2008).

[56] W. H. Furry, Phys. Rev. **51**, 125 (1937).

[57] J. J. van der Bij and E. W. N. Glover, Nucl. Phys. **B313**, 237 (1989).

[58] W. Buchmuller and D. Wyler, Nucl. Phys. **B268**, 621 (1986).

[59] T. Hahn, Comput. Phys. Commun. **140**, 418 (2001); T. Hahn and M. Perez-Victoria, Comput. Phys. Commun. **118**, 153 (1999).

[60] J. Alwall, P. Demin, S. de Visscher, R. Frederix, M. Herquet, F. Maltoni, T. Plehn, D. L. Rainwater, and T. Stelzer, J. High Energy Phys. 09 (2007) 028.

[61] H. Murayama, I. Watanabe, and K. Hagiwara, KEK Report No. 91-11, 1992.

[62] G. J. van Oldenborgh, Comput. Phys. Commun. **66**, 1 (1991).

[63] S. Brandt, C. Peyrou, R. Sosnowski, and A. Wroblewski, Phys. Lett. **12**, 57 (1964); E. Fahri, Phys. Rev. Lett. **39**, 1587 (1977).

[64] CMS Collaboration, Phys. Lett. B **699**, 48 (2011).

[65] S. Catani, G. Turnock, and B. R. Webber, Phys. Lett. B **295**, 269 (1992); Y. L. Dokshitzer, A. Lucenti, G. Marchesini, and G. P. Salam, J. High Energy Phys. 01 (1998) 011.

[66] A. Heister *et al.* (ALEPH Collaboration), Eur. Phys. J. C **35**, 457 (2004); J. Abdallah *et al.* (DELPHI Collaboration), Eur. Phys. J. C **37**, 1 (2004); P. Achard *et al.* (L3 Collaboration), Phys. Rep. **399**, 71 (2004).

[67] A. Gehrmann-De Ridder, T. Gehrmann, E. W. N. Glover, and G. Heinrich, Phys. Rev. Lett. **99**, 132002 (2007); T. Becher and M. D. Schwartz, J. High Energy Phys. 07 (2008) 034.